ACS OMEGA

http://pubs.acs.org/journal/acsodf

Article

Novel Strategy for Gallium-Substituted Hydroxyapatite/*Pergularia daemia* Fiber Extract/Poly(*N*-vinylcarbazole) Biocomposite Coating on Titanium for Biomedical Applications

Saravanakumar Ponnusamy, Ramya Subramani, Shinyjoy Elangomannan, Kavitha Louis, Manoravi Periasamy, and Gopi Dhanaraj*

Cite This: *ACS Omega* 2021, 6, 22537−22550

Read Online

ACCESS | Metrics & More | Article Recommendations

ABSTRACT: The current work mainly focuses on the innovative nature of nano-gallium-substituted hydroxyapatite (nGa-HAp)/*Pergularia daemia* fiber extract (PDFE)/poly(*N*-vinylcarbazole) (PVK) biocomposite coating on titanium (Ti) metal in an eco-friendly and low-cost way through electrophoretic deposition for metallic implant applications. Detailed analysis of this nGa-HAp/PDFE/PVK biocomposite coating revealed many encouraging functional properties like structure and uniformity of the coating. Furthermore, gallium and fruit extract of PDFE-incorporated biocomposite enhance the *in vitro* antimicrobial, cell viability, and bioactivity studies. In addition, the mechanical and anticorrosion tests of the biocomposite material proved improved adhesion, hardness, and corrosion resistance properties, which were found to be attributed to the presence of PDFE and PVK. Also, the swelling and degradation behaviors of the as-developed material were evaluated in simulated body fluids (SBF) solution. The results revealed that the as-developed composite exhibited superior swelling and lower degradation properties, which evidences the stability of composite in the SBF solution. Overall, the results of the present study indicate that these nGa-HAp/PDFE/PVK biocomposite materials with improved mechanical, corrosion resistance, antibacterial, cell viability, and bioactivity properties appear as promising materials for biomedical applications.

INTRODUCTION

Developing novel bioactive materials with multifunctionality for orthopedic application is one of the most important dynamic research areas in the materials science field for scientific growth in the 21st century.[1,2] During the last few decades, artificial orthopedic substitutes gained more importance due to the increase in bone defects and joint degradation because of the aging population in the world.[3] The requirement for the fabrication of metallic implants for load-bearing orthopedic applications is increased. Ti and its alloys are widely used metallic implant materials for orthopedic applications due to their commendable fatigue properties, high strength, low wear rate, nontoxicity, and biocompatibility.[4,5] However, owing to its lack of osteoconductive and osteoinductive properties and also inherent bioinertness, dynamic research was mainly focused on the surface modification of the Ti metal implants using HAp-based bioceramic coating.[6]

In recent years, HAp-based coatings have been appraised and developed as the most potential material for orthopedic applications.[7] HAp is one of the most popular biomaterials, and it is mainly used in various biomedical applications due to its high osteoconductivity and excellent biodegradability.[8] Owing to its immense properties and similarity to natural bone, biomaterials based on HAp are widely used in various biomedical applications in the form of bone fillers, coating material for metallic implants, etc.

However, most of them were found to have potential toxicity issues in this area. The investigation of the bioactive and biocompatible materials such as HAp for various health care applications are still going on as a combined effort of chemists, biologists, physicists, and engineers.[9,10] The cost of production is the main issue for the chemical syntheses of HAp as it involves using expensive chemicals. Hence, to reduce the production cost for the synthesis of HAp, different biogenic

Received: April 25, 2021
Accepted: August 13, 2021
Published: August 24, 2021

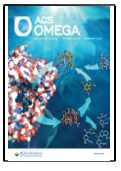

materials such as coral, eggshells, seashells, freshwater shells, and bovine bones are widely used as calcium sources.[11]

Among the above-mentioned biogenic waste, *Gastropoda* shells are easily available in nature and are found to contain plenty of calcium carbonate, which can be used as a calcium source for the synthesis of HAp. Further, it has been also shown that natural HAp obtained from the natural source has better bioactivity compared to chemically synthesized HAp bioceramic materials.[12,13] In addition to this, some biological/structural performances of pure HAp such as implantation efficacy, osseointegration ability, *in vivo* degradation rate, and antibacterial properties were improved by modifying the composition through substitution or doping small amounts of foreign ions for a variety of applications.[14] However, nanosized synthetic HAp particles are very closely similar to the HAp crystals in human natural bone.[15]

Inspired by the limitation of pure HAp and benefits of nanosized HAp particles, we undertook this research. The employment of plant extract for the fabrication of nano synthetic HAp has received increasing attention owing to the absence of toxic chemicals.[16,17] In the last few years, a growing number of plants have been mainly used for rapid extracellular and efficient synthesis of HAp.[18−20] Among the plant extracts, the extracts of *Chomelia asiatica*, *Sida acuta*, *Azadirachta indica*, and *Gmelina asiatica* are cheap and eco-friendly. Among the plant extracts, *Azadirachta indica* gum was used as the template for the synthesis of nano HAp biomaterials.[21] On the other hand, the antibacterial property of pure HAp is limited. Generally, the infection usually occurs after surgery and can lead to implant rejection. Hence, the antibacterial property of HAp is modified through a small amount of substituting (or) doping of ions for various applications. Recently, several ions have been incorporated in HAp, such as La^{3+}, Ce^{3+}, Yt^{3+}, Ga^{3+}, etc., which were subjected to Ca^{2+} substitution within the HAp matrix.[22−26]

These trivalent ions can affect the biocompatibility, cell attachment toward the biological cells, and antibacterial property. Among the trivalent metal ions, gallium (Ga^{3+}) is the most beneficial trace ion, which decreases the bacterial infections of the human body. Hence, these more interesting facts triggered the recent research of substituting Ga^{3+} with HAp.[27,28]

Apatite-containing Ga^{3+} has exhibited antibacterial effects under both *in vivo* and *in vitro* conditions. Moreover, Ga^{3+} is the most beneficial trace ion due to its strong affinity to bone tissues and inhibits bone resorption, which is mainly used in biomedical applications.[29,30] In addition, Ga^{3+} exhibits outstanding antibacterial activity and is supposed to play a vital role in the acceptance of orthopedic implants.[30] Furthermore, it has been proposed that substitution of Ga^{3+} in HAp composition has an important result over pure HAp. The biological properties of Ga-substituted HAp (Ga-HAp) can be further enhanced by the addition of suitable reinforcing material. For this purpose, recently, young researchers are working on the reinforcing of different natural and synthetic fibers.[31] The employment of plant extract has received increasing attention over chemical- and microbial-based materials because it involves using exclusive chemicals.[32,33]

Generally, plants and plant extracts have long been used in medical applications mainly due to the presence of bioactive polyphenolic compounds, which may be stored in plant parts such as leaves, roots, fruits, and seeds. Hence, different plants have been studied using recent scientific approaches to classify various biological compounds of these medicinal plants.[34,35] *Pergularia daemia* (forsk, family *Asclepiadaceae*) is native to Asia, and it grows in plains of hotter regions of India, which is commonly known as "Veliparuthi" in Tamil Nadu. The excellent antidiabetic, hepatoprotective, anti-inflammatory, and cardiovascular effects of this natural medicinal plant have been reported in Ayurvedic and folk medicine.[36,37] Since there is no individual bioactive material available to fulfill all of the essential requirements for biomedical applications, fabrication of composite as an attractive for human bone issues has become mandatory. Hence, these attractive facts triggered the recent work, which focuses on the (PDFE) combined with nGa-HAp material. Recent research is mainly directed toward the mixing of polymers with inorganic materials, which exhibit outstanding features with homogeneous mechanical properties. The addition of an electroactive polymer to the nGa-HAp/PDFE at an ambient temperature reduces its brittleness.

Alternatively, nGa-HAp/PDFE composite combined with electroactive polymers offers better dispersion and can prospectively enhance (or) maintain the same bioactive and antibacterial properties of the nGa-HAp/PDFE composite material, while providing a mechanical, broad range of structural and degradation properties. Unfortunately, a handful of studies about the mechanical behavior of electroactive polymer in nGa-HAp/PDFE composite are available. None of them have investigated the possibility of using these ternary composites as robust coating materials to resist biofilm formation on metallic implants. Generally, electroactive polymers are an excellent selection for such composite owing to their anticorrosion properties.[38−40] Among the electroactive polymers, poly(*N*-vinylcarbazole) (PVK) is an excellent candidate because of its superior mechanical and thermal properties.[40] Inspired by the limitations of other polymers and benefits of PVK, we undertake this research work. Hence, in this paper, we report on the fabrication of nGa-HAp/PDFE/PVK composite on Ti by electrophoretic deposition method and the investigation of its structural, morphological, mechanical, and corrosion stability, as well as *in vitro* biocompatibility. Multifunctional Ti implant surface that simultaneously suppresses bacteria growth and enhances biocompatibility as well as mechanical strength may be achieved by combining the components such as nGa-HAp, PDFE, and PVK in composite coatings. This approach has been used recently to develop composite coating using pulsed laser deposition, electrophoretic deposition, plasma spray, electrodeposition, etc.[41−45]

Among these techniques, electrophoretic deposition (EPD) is an intensively used technique to deposit composite coating on Ti implant since it is the most established technique compared to others deposition techniques. The EPD technique recommends the attractive prospect to produce homogeneous and dense polymer, fiber, ceramic, and composite coatings at a reduced cost and high mechanical strength for biomedical applications. The electrophoretic deposition technique provides suspension stability, and the result of these approaches is a nGa-HAp/PDFE/PVK composite coating that either has PDFE extract and PVK dispersed in a surrounding nGa-HAp matrix. With this in mind, we fabricated multifunctional nGa-HAp/PDFE/PVK composite from an eco-friendly and low-cost material acting as the main source with outstanding antibacterial activity, biocompatibility, and enhanced mechanical properties for biomedical applications.

https://doi.org/10.1021/acsomega.1c02186
ACS Omega 2021, 6, 22537−22550

RESULTS AND DISCUSSION

FT-IR Analysis. The FT-IR spectra of HAp, Ga-HAp, nGa-HAp, nGa-HAp/PDFE, and nGa-HAp/PDFE/PVK coating on Ti samples are shown in Figure 1a–e. The illustrative peaks

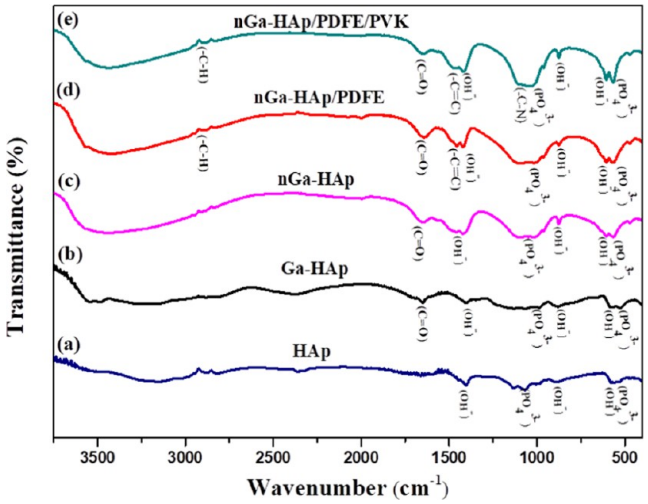

Figure 1. FT-IR spectra of (a) HAp, (b) Ga-HAp, (c) nGa-HAp, (d) nGa-HAp/PDFE, and (e) nGa-HAp/PDFE/PVK composites.

observed in Figure 1b correspond to Ga-HAp coating, in which the absorption peaks are clearly observed at 540, 591, 885, and 1006 cm^{-1} that correspond to the phosphate (PO_4^{3-}) groups. Further, the presence of stretching mode of hydroxyl (OH^-) group was confirmed at 631 cm^{-1}.[15] The FT-IR peaks for Ga-HAp showed a slight shift in the peak positions (Figure 1b) compared with the standard peaks for pure HAp (Figure 1a),[15] which evidences the substitution of Ga^{3+} into the Ca^{2+} lattice in pure HAp sample. The FT-IR peaks observed for the nGa-HAp coating (Figure 1c) showed that mediated synthesis does not influence any major changes in PO_4^{3-} and OH^- groups except the slight variation of peaks in Ga-HAp coating. Apart from the typical nGa-HAp peaks, the absorption peaks appearing at 3016 and 1458 cm^{-1} are attributed to the stretching of C–H and C=C groups in the PDFE (Figure 1d), respectively.[37] All of these characteristic peaks clearly evidence the formation of both nGa-HAp and PDFE units in the nGa-HAp/PDFE composite. The spectrum obtained at PVK incorporated into nGa-HAp/PDFE composite coating is shown in Figure 1e. The FT-IR spectrum shows the peaks attributable to the nGa-HAp/PDFE composite coating, and in addition, the characteristic peak at 1818 cm^{-1} reveals the stretching of the C–N group, indicating the presence of PVK polymer in the nGa-HAp/PDFE matrix.[38]

All of the above illustrative peaks imply that the nGa-HAp/PDFE/PVK composite coatings contain both the PDFE and PVK units. Thus, in this FT-IR study, the presence of both the PDFE and PVK units strongly reveals the formation of nGa-HAp/PDFE/PVK composite coatings on Ti sample (Figure 1e).

XRD Analysis. Phase analysis of the HAp, Ga-HAp, nGa-HAp, nGa-HAp/PDFE, and nGa-HAp/PDFE/PVK coating on Ti samples was carried out by XRD, as depicted in Figure 2a–e. The representative XRD pattern of Ga-HAp sample is depicted in Figure 2b, where the peaks appearing at 2θ values of 25.78, 31.52, 32.7, 35.9, 39.64, 46.52, 49.34, and 53.4° were found in the Ga-HAp matrix. The peaks identified for Ga-HAp

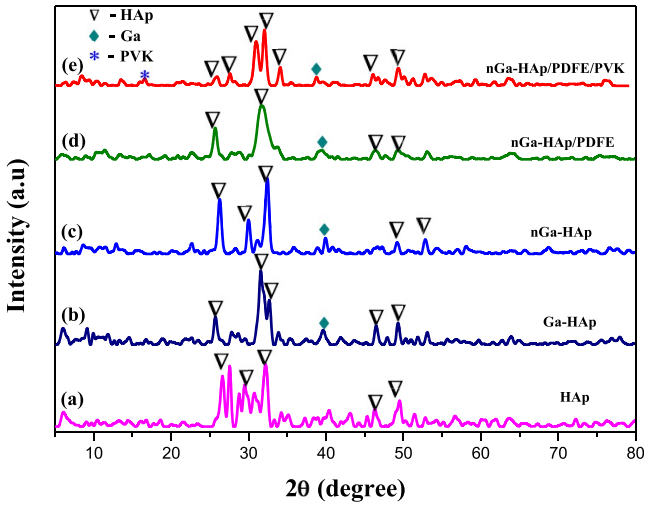

Figure 2. XRD spectra of (a) HAp, (b) Ga-HAp, (c) nGa-HAp, (d) nGa-HAp/PDFE, and (e) nGa-HAp/PDFE/PVK composites.

are matching well with the International Centre for Diffraction Data (ICDD card no. 09-0432) of pure HAp sample (Figure 2a).[15,23] Hence, the formed Ga-HAp sample has a hexagonal crystal structure. In the case of substitution of ions, the ionic radius of gallium ions (0.62 Å) is low compared to that of Ca^{2+} (0.99 Å), and hence it can more easily substitute Ca^{2+} and take part in the formation of a compound in the HAp matrix with electrostatic interactions. It is also more evident that there is a nonexistence of any other secondary phases, which are generally seen during the formation of the Ga-HAp matrix.

Hence, the substitution of Ca^{2+} by Ga^{3+} takes place more simply and effectively without changing the crystal structure of the HAp matrix. The XRD peaks observed for the nGa-HAp coating (Figure 2c) showed slight variation of peaks in Ga-HAp coating. The *Azadirachta indica* gum mediator does not change the 2θ values of the nGa-HAp coating appreciably. Hence, similar XRD peaks have been obtained for nGa-HAp and Ga-HAp coating (Figure 2b,c). The illustrative broad and intense peaks (Figure 2d) are observed at 2θ values of 25.66, 31.7, 38.94, 46.26, 49.22, and 53.4°, which strongly designates the formation of nGa-HAp/PDFE composite.[34,35]

In the XRD patterns for the nGa-HAp/PDFE/PVK composite sample (Figure 2e), a broad peak and amorphous nature of nGa-HAp/PDFE/PVK composite exist along with the diffraction peaks for PVK, which clearly shows that the nGa-HAp/PDFE/PVK composite had a more ordered arrangement than the single compound due to the presence of Ga-HAp. Moreover, strong diffraction peaks were located at a 2θ value of 21.76°, which revealed face-to-face ordered structure of PVK present in the nGa-HAp/PDFE/PVK composite.[38] In addition to this, XRD patterns show that the nGa-HAp coating strongly influenced the crystalline behavior of the nGa-HAp/PDFE/PVK composite. As shown in Figure 2e, the XRD patterns of the nGa-HAp/PDFE/PVK composite show that no significant typical interfacial phases were formed or lost with the addition of PDFE and PVK, which strongly advocates the successful formation of nGa-HAp/PDFE/PVK composite sample.

HRSEM Analysis. The properties of nGa-HAp, PDFE, and PVK samples are strongly dependent on their structure and morphology. Representative HRSEM micrographs of HAp, Ga-HAp, nGa-HAp, nGa-HAp/PDFE, and nGa-HAp/PDFE/

https://doi.org/10.1021/acsomega.1c02186
ACS Omega 2021, 6, 22537–22550

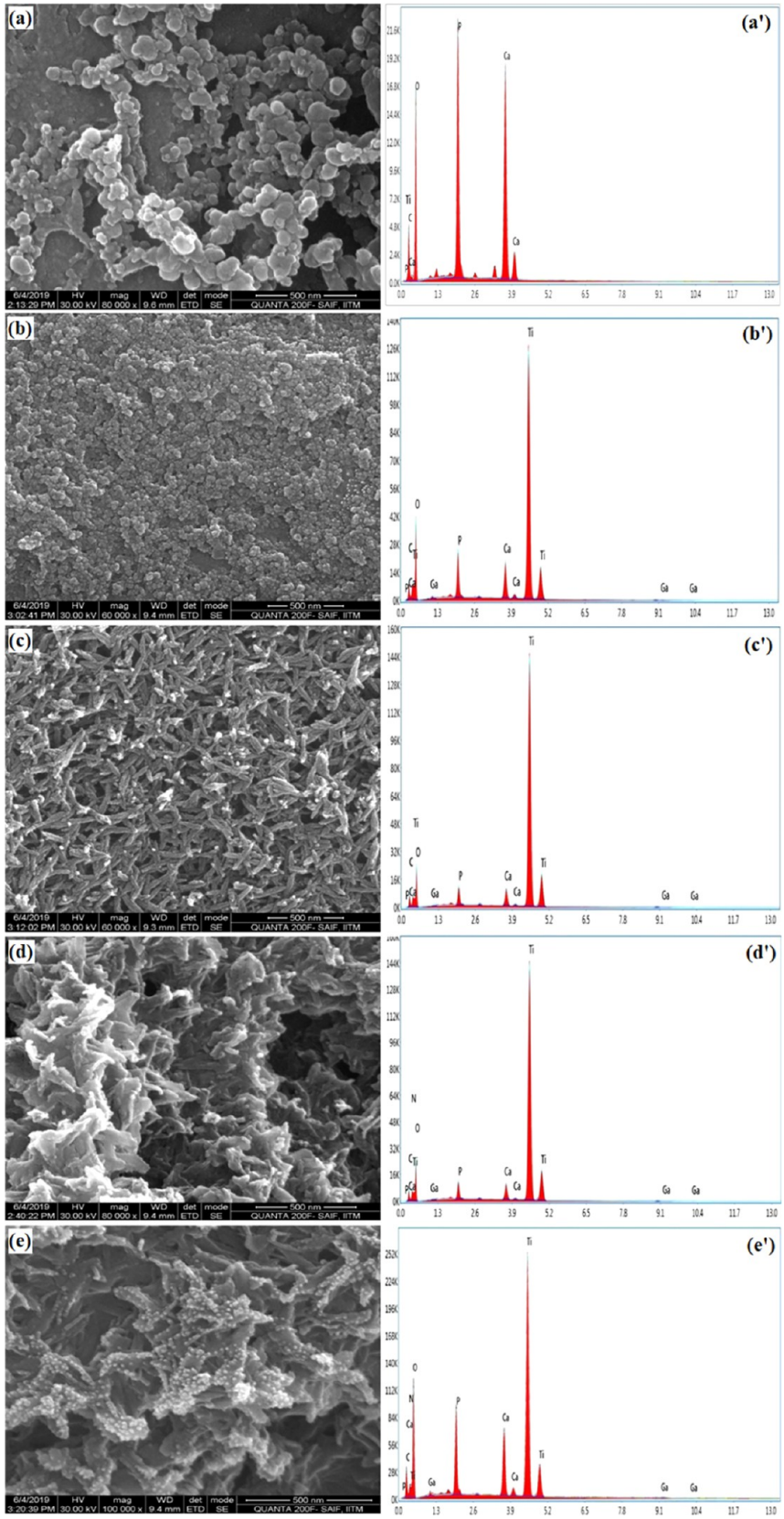

Figure 3. HRSEM morphology and elemental composition of (a, a′) HAp, (b, b′) Ga-HAp, (c, c′) nGa-HAp, (d, d′) nGa-HAp/PDFE, and (e, e′) nGa-HAp/PDFE/PVK composite coating on Ti.

PVK coating on Ti samples are displayed in Figure 3a−e, and their corresponding elemental compositions are more clearly depicted in Figure 3a′−e′. The surface morphology of the HAp-coated Ti (Figure 3a) exhibited the formation of irregular agglomerated granular-like structure. The Ga-HAp coating obtained without PDFE and PVK, shown in Figure 3b, display

https://doi.org/10.1021/acsomega.1c02186
ACS Omega 2021, 6, 22537−22550

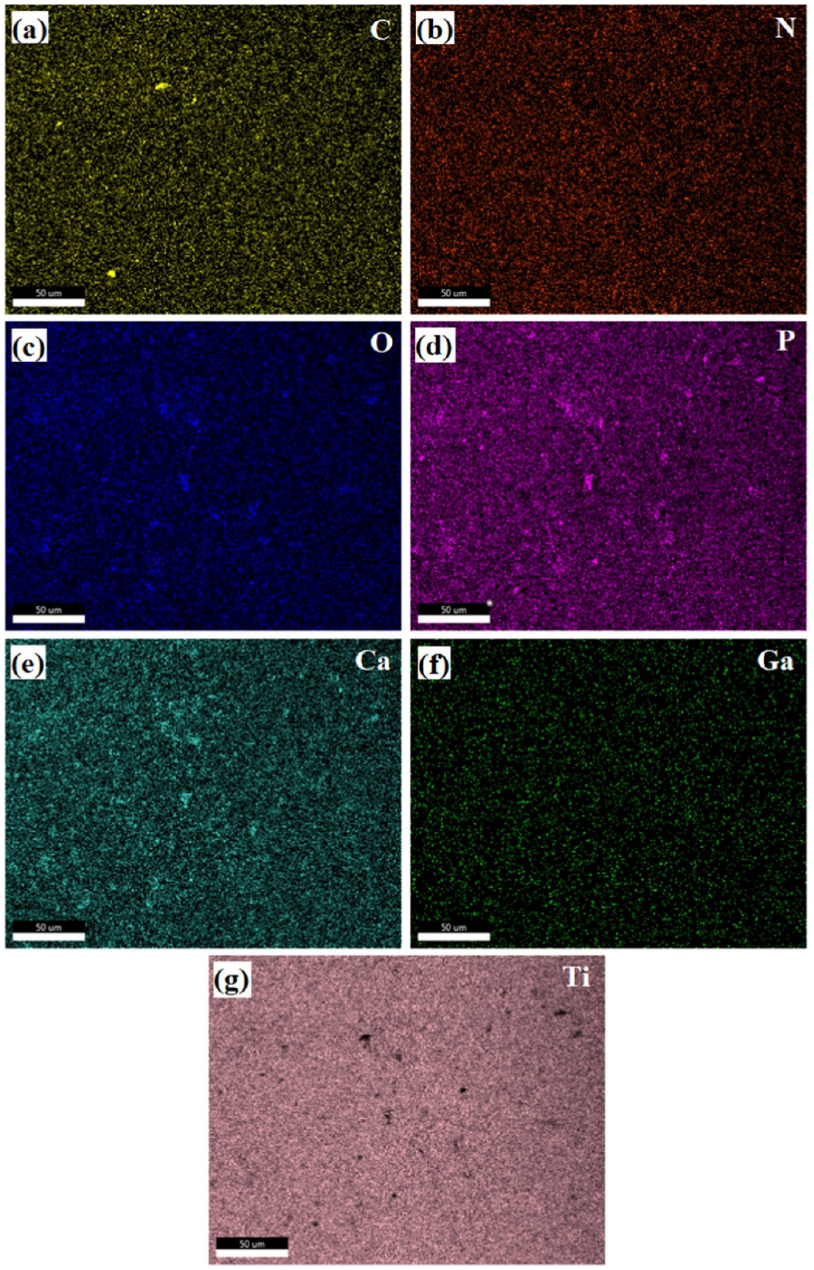

Figure 4. Elemental mapping images of the distribution of (a) C, (b) N, (c) O, (d) P, (e) Ca, (f) Ga, and (g) Ti ions for nGa-HAp/PDFE/PVK coating on Ti.

the granular-like morphology with irregular pores, and thus the coating was rough and irregular in nature. Figure 3c represents the morphology of nGa-HAp-coated Ti, which displays the formation of nanorods. After PDFE were introduced into the nGa-HAp/PDFE composite coating, the typical interconnected and agglomerated rod-like morphology still dominated in the nGa-HAp/PDFE composite coatings as seen from Figure 3d.

The HRSEM micrographs of nGa-HAp/PDFE composite coatings revealed a slight difference with incorporation of PDFE in the nGa-HAp unit. It is inferred that the presence PDFE in nGa-HAp/PDFE composite matrix causes the fabrication of a uniform composite coating with less porous and finer morphology, leading to increasing compactness of the nGa-HAp coatings. It has been reported that the growth of white spherical grains was the result of PDFE interaction with the nGa-HAp during the electrophoretic deposition.

Further, the reinforcement of PVK in the nGa-HAp/PDFE composite matrix clearly shows that the nGa-HAp/PDFE/PVK composite-coated Ti surface (Figure 3e) exhibited a uniform and more compact morphology with rod and white spherical grain morphology all over the Ti surface without any pores in nature.

The EDS analysis of the HAp, Ga-HAp, nGa-HAp, nGa-HAp/PDFE, and nGa-HAp/PDFE/PVK coating on Ti samples is shown in Figure 3a′−e′. In Figure 3a′, the HAp coatings on Ti reveals the presence of Ca, O, P, N, and Ti. The intense peaks for Ga, Ca, P, Ti, and O (Figure 3b′,c′) confirm the formation of Ga-HAp and nGa-HAp, whereas the nGa-HAp/PDFE composite coating (Figure 3d′) showed the presence of Ga, Ca, P, N, O, and Ti. Figure 3e′ shows the

https://doi.org/10.1021/acsomega.1c02186
ACS Omega 2021, 6, 22537−22550

EDS spectrum of the nGa-HAp/PDFE/PVK composite-coated sample, which reveals the presence of C, N, O, P, Ca, and Ga, thereby confirming the existence of nGa-HAp/PDFE/PVK composite coating on Ti.

Figure 4a–g shows the elemental mapping of nGa-HAp/PDFE/PVK composite coating on Ti, which indicated the presence of C, N, O, P, Ca, Ga, and Ti ions. The homogeneous distribution of mineral ions was supported by the elemental mapping results.

Vickers Micro-Hardness. Any metallic implant that is to be used for orthopedic implant application must be tested for its hardness, which is the most significant parameter to be followed before implantation. The Vickers micro-hardness (H_v) gives significant information about load-bearing tendency when it is implanted into the human body. The H_v values obtained for the as-developed HAp, Ga-HAp, nGa-HAp, nGa-HAp/PDFE, and nGa-HAp/PDFE/PVK composite-coated Ti samples using the Vickers micro-hardness test are depicted in Figure 5a–e. The H_v values observed for the HAp, Ga-HAp, and nGa-HAp are found to be 341.4, 345.6, and 348.2H_v, respectively.

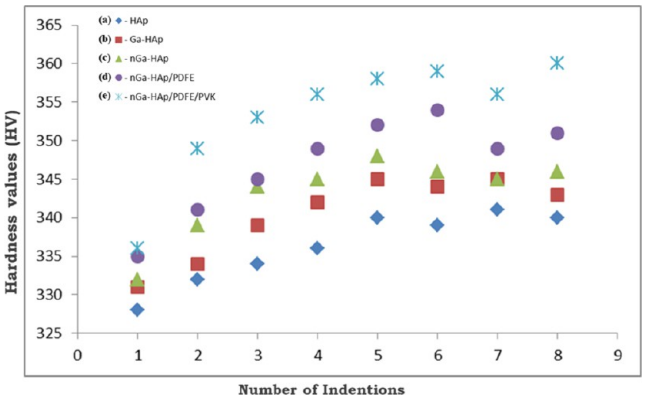

Figure 5. Vickers micro-hardness of (a) HAp, (b) Ga-HAp, (c) nGa-HAp, (d) nGa-HAp/PDFE, and (e) nGa-HAp/PDFE/PVK composite-coated Ti sample.

However, when PDFE is incorporated, the H_v value is found to be slightly higher (354.5H_v) than the other HAp coatings. Similarly, the nGa-HAp/PDFE/PVK composite sample showed 360.4H_v which is greater than that of the nGa-HAp/PDFE-, nGa-HAp-, Ga-HAp-, and HAp-coated Ti samples. An interesting observation is that the hardness increased upon the incorporation of PDFE and PVK. The hardness value may also be attributed due to the uniform and more compact coating morphology of the composite. Thus, the obtained hardness value for nGa-HAp/PDFE/PVK composite-coated Ti will make it suitable for load-bearing orthopedic applications.

Potentiodynamic Polarization Studies. The corrosion protection performance of the blank Ti, Ga-HAp, nGa-HAp, nGa-HAp/PDFE, and nGa-HAp/PDFE/PVK composite-coated Ti samples was studied for long-term applications. To reveal the protection ability of the nGa-HAp/PDFE/PVK composite coating, a polarization study was performed in SBF medium, and the corresponding polarization curve is presented in Figure 6. From the recorded polarization curves, the Tafel region was identified and extrapolated to corrosion potential (E_{corr}) to get corrosion current (i_{corr}), and the obtained corrosion parameters are given in Table 1.

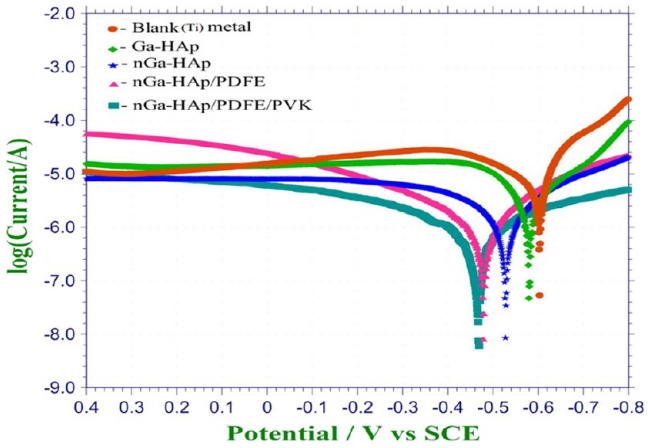

Figure 6. Potentiodynamic polarization curves of blank (Ti) and Ga-HAp, nGa-HAp, nGa-HAp/PDFE, and nGa-HAp/PDFE/PVK coating on Ti samples obtained in SBF solution.

Table 1. Electrochemical Parameters of the Blank (Ti) and Ga-HAp-, nGa-HAp-, nGa-HAp/PDFE-, and nGa-HAp/PDFE/PVK-Coated Ti in SBF Solution

sample code	E_{corr} (mV vs SCE)	i_{corr} (μA/cm^2)
blank (Ti)	−618.7 ± 5.1	2.51 ± 0.9
Ga-HAp	−596.6 ± 3.2	1.32 ± 0.5
nGa-HAp	−545.0 ± 4.4	0.38 ± 0.09
nGa-HAp/PDFE	−496.2 ± 8.2	0.25 ± 0.04
nGa-HAp/PDFE/PVK	−452.4 ± 6.3	0.10 ± 0.06

The polarization curves of Ga-HAp- and nGa-HAp-coated Ti exhibited E_{corr} values of −596.6 ± 3.2 and −545.0 ± 4.4 mV, respectively, which was found to have a higher electropositive value compared to the E_{corr} value of blank Ti (−618.7 ± 5.1 mV). However, the polarization curves of composite (nGa-HAp/PDFE and nGa-HAp/PDFE/PVK)-coated Ti showed a slight shift toward more positive direction (i.e., −496.2 ± 8.2 and −452.4 ± 6.3 mV) than the Ga-HAp- and nGa-HAp-coated Ti. Thus, among the attained polarization curves, nGa-HAp/PDFE/PVK composite-coated Ti exhibited a maximum shift of corrosion potential (E_{corr} = −452.4 ± 6.3 mV), which clearly reveals the higher corrosion protection performance of Ti. Similarly, the current density (i_{corr} = 0.10 ± 0.06 μA/cm^2) for nGa-HAp/PDFE/PVK composite-coated Ti was found to decreased (Table 1) in the following order:

Blank (Ti) > Ga-HAp > nGa-HAp > nGa-HAp/PDFE > nGa-HAp/PDFE/PVK.

Among the coatings, the composite-coated Ti with compact grainlike morphology over the Ti proves to be more corrosion resistant than other coatings. Thus, from the polarization curves, it is evident that the nGa-HAp/PDFE/PVK composite-coated Ti has the noblest corrosion potential value and the lowest corrosion current density, which reports the greater stability of the composite-coated Ti. Thus, the investigation of polarization plots showed a maximum shift of corrosion values for nGa-HAp/PDFE/PVK composite-coated Ti toward the noble direction, which strongly indicates that the composite-coated Ti revealed the maximum corrosion protection ability in SBF solution, i.e., composite-coated Ti is stable in physiological solution and enhance the lifetime of the implant for long-term orthopedic applications.

https://doi.org/10.1021/acsomega.1c02186
ACS Omega 2021, 6, 22537−22550

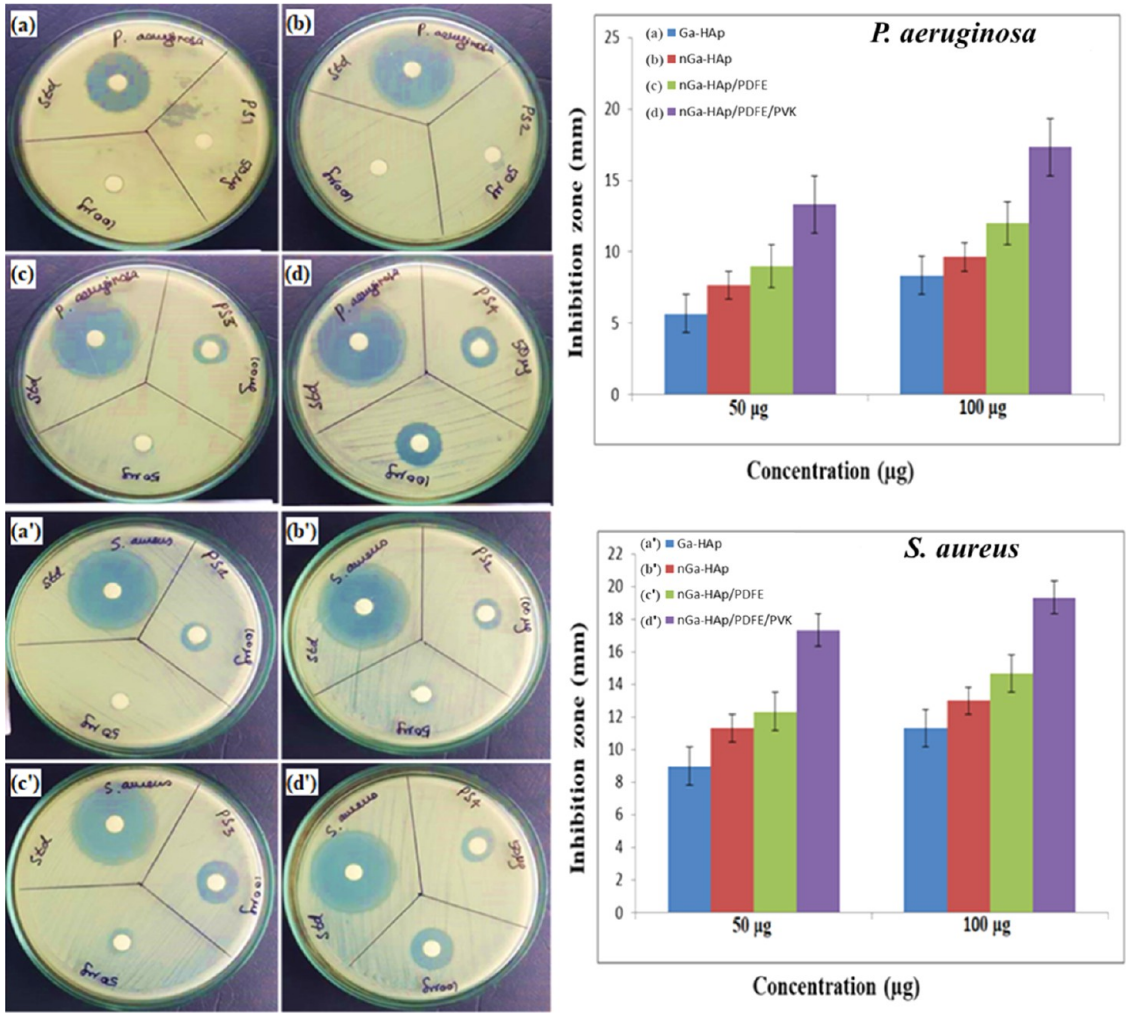

Figure 7. Antibacterial activity of (a, a′) Ga-HAp, (b, b′) nGa-HAp, (c, c′) nGa-HAp/PDFE, and (d, d′) nGa-HAp/PDFE/PVK composites at 50 and 100 μg against *P. aeruginosa* and *S. aureus* bacteria.

Antibacterial Activity. The antibacterial performance of Ga-HAp, nGa-HAp, nGa-HAp/PDFE, and nGa-HAp/PDFE/PVK composite samples was tested against Gram-negative strain *P. aeruginosa* and Gram-positive strain *S. aureus* that are responsible for implant-related infections. The inhibition zones of the as-developed materials at 50 and 100 μL against *P. aeruginosa* and *S. aureus* are shown in Figure 7. Among the samples, the nGa-HAp/PDFE/PVK composite sample exhibited a higher zone of inhibition against *P. aeruginosa* and *S. aureus*, i.e., 13 and 17 mm for 50 μL, and 17 and 19 mm for 100 μL volumes, respectively. The results exhibited that the presence of Ga in HAp and PDFE in the composite is responsible for the antibacterial property of the composite (Table 2).

The mechanism involves the interaction of the nGa-HAp/PDFE/PVK composite with proteins and enzymes of bacteria. Due to this interaction, there occur structural damages in the cell wall and bacterial membrane, thereby preventing bacterial reproduction. Also, from the result (Figure 7), it is observed that the zone of inhibition obtained for the composite sample against *P. aeruginosa* (Figure 7a–d) is higher than that obtained for *S. aureus* (Figure 7a′–d′), which may be due to the structural difference of cell wall membrane of Gram-negative and Gram-positive bacteria.

Table 2. Antibacterial Activity of Ga-HAp, nGa-HAp, nGa-HAp/PDFE, and nGa-HAp/PDFE/PVK Composites at 50 and 100 μg against *P. aeruginosa* and *S. aureus*

bacterial strain	sample	inhibition zone (mm) mean ± SD (50 μg)	inhibition zone (mm) mean ± SD (100 μg)
P. aeruginosa	Ga-HAp	5.66 ± 1.52	8.33 ± 1.15
	nGa-HAp	7.66 ± 1.52	9.66 ± 0.57
	nGa-HAp/PDFE	9 ± 1.73	12 ± 1
	nGa-HAp/PDFE/PVK	13.33 ± 0.57	17.33 ± 1.52
S. aureus	Ga-HAp	9 ± 1	11.33 ± 1.15
	nGa-HAp	11.33 ± 0.57	13 ± 1
	nGa-HAp/PDFE	12.33 ± 1.15	14.66 ± 0.57
	nGa-HAp/PDFE/PVK	17.33 ± 0.57	19.33 ± 0.57

These structural differences show a substantial increase in permeability, making the organism incompetent of regular functions and, finally, causing cell death.

***In Vitro* Cell Viability Test.** The viabilities of MG-63 osteoblast cells on the nGa-HAp/PDFE/PVK composite determined using MTT assay at different concentrations of 0.5, 5, 50, 100, and 150 μg are shown in Figure 8. The bar diagram indicates that the nGa-HAp/PDFE/PVK composite exhibited a statistically significant increase in the cellular

https://doi.org/10.1021/acsomega.1c02186
ACS Omega 2021, 6, 22537−22550

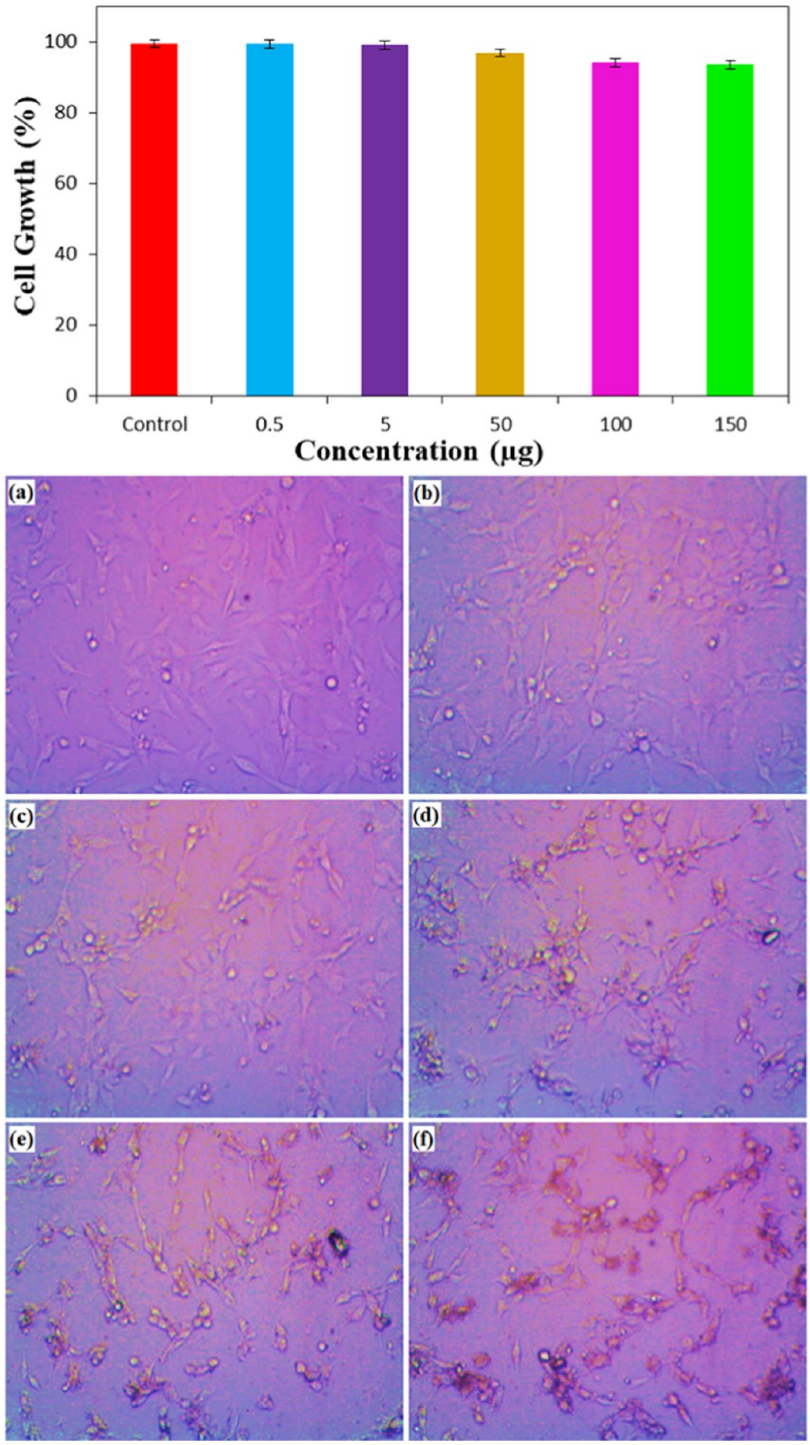

Figure 8. % Cell viability and optical microscopic images of MG63 cells on the nGa-HAp/PDFE/PVK composite coating at (a) control, (b) 0.5 μg, (c) 5 μg, (d) 50 μg, (e) 100 μg, and (f) 150 μg.

viability with increasing concentration of the samples from 0.5 to 150 μg compared with the control ($p < 0.05$). However, the increase in the viability of the cells over the nGa-HAp/PDFE/PVK composite-coated sample above 90% implied a higher proliferation rate of the cells, which may be due to the presence of Ga^{3+} in the composite sample. The obtained bar diagram is in good agreement with the optical microscopic images.

The optical microscopic cell viabilities of MG-63 osteoblast cells on the nGa-HAp/PDFE/PVK composite determined using MTT assay at various concentrations of 0.5, 5, 50, 100, and 150 μg are shown in Figure 8b–f. As verified by MTT assay, the proliferation of MG-63 cells increased appreciably at different concentrations. From Figure 8c, more viable cells were observed on 5 μg of the nGa-HAp/PDFE/PVK composite sample while comparing the cell viability on the composite at 0.5 μg. On increasing the concentration from 0.5 to 100 μg, the viability of MG-63 osteoblast cells was higher at the 100 μg concentration of nGa-HAp/PDFE/PVK composite coatings.

https://doi.org/10.1021/acsomega.1c02186
ACS Omega 2021, 6, 22537−22550

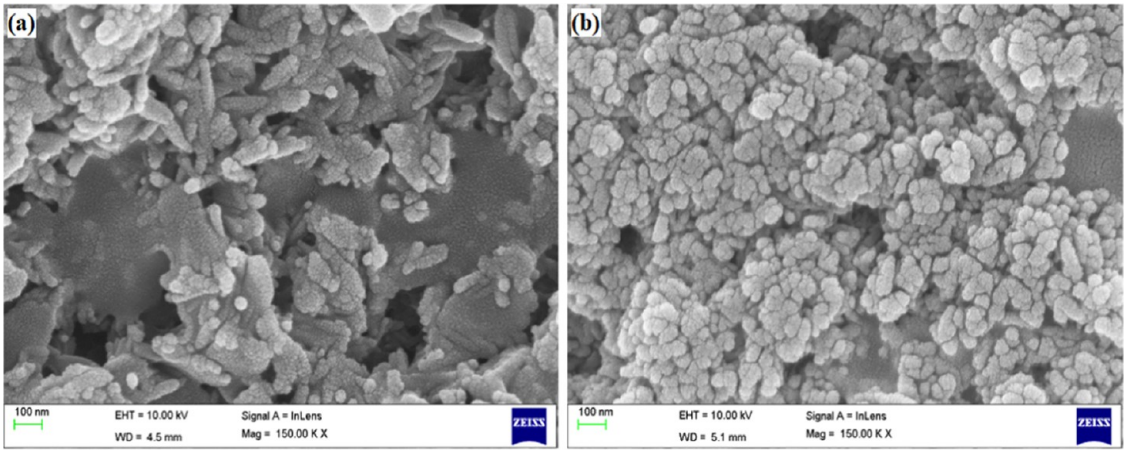

Figure 9. FESEM images of SBF growth on nGa-HAp/PDFE/PVK composite coating on Ti at (a) 7 days and (b) 14 days.

Correspondingly, the % of MG-63 viable cells were extensively increased for 150 μg on the nGa-HAp/PDFE/PVK composite. For all of the concentrations, the examined % cell viability nGa-HAp/PDFE/PVK composite was exhibiting superior growth similar to the control owing to the compact morphology of the sample, and this supports the nontoxic scenery of the nGa-HAp/PDFE/PVK composite. Thus, the as-developed nGa-HAp/PDFE/PVK composite is imperative for the enhancement of the cell viability nature on the Ti implant.

***In Vitro* Bioactivity.** The *in vitro* apatite ability of the nGa-HAp/PDFE/PVK composite-coated Ti samples after 7 and 14 days of immersion in SBF is shown in Figure 9a,b. The surface of the nGa-HAp/PDFE/PVK composite-coated samples exhibited apatite formation at 7 and 14 days of immersion in SBF, but the surface coverage and the growth of apatite formation differ each day. On day 7, the apatite formation on the surface is found as granule-like apatite structure, which is well clear from Figure 9a. On increasing the immersion period to 14 days (Figure 9b), an improved formation of dense apatite layer with more granule-like morphology was observed on the nGa-HAp/PDFE/PVK composite-coated Ti surface.

As a result, the surfaces were completely covered with dense HAp and the formation increased with days from 7 to 14 days, which strongly evidences that the nGa-HAp/PDFE/PVK composite-coated samples accelerate the biomineralization process in the SBF solution. Generally, the Ca-rich positively charged surface can be easily attracted by the negatively charged (OH^- and PO_4^{3-}) ions in the SBF to form amorphous Ca-poor apatite layer, which leads to the formation of apatite layer on the nGa-HAp/PDFE/PVK composite-coated Ti samples. Thus, from the FESEM morphologies, it is clearly manifested that the apatite-forming ability at 7 and 14 days of immersion and the resultant nGa-HAp/PDFE/PVK composite coating exhibited the enhanced bioactivity in SBF solution.

Swelling and Degradation Behaviors in SBF. To widen the application of the as-developed composite in the field of medicine, the swelling and degradation behaviors were observed in SBF solution. Also to ensure the nontoxic and bioactive nature of the as-developed composite, the swelling was performed in SBF, which is similar to human blood plasma.

It is also very important to note that if any material is too stiff, there occurs the lack of adherence between the composite coating and the implant. In general, the presence of HAP in the composite provides superiority on the swelling behavior. The swelling behavior of all of the samples is shown in Figure 10. The results indicated that the swelling percentage increased up

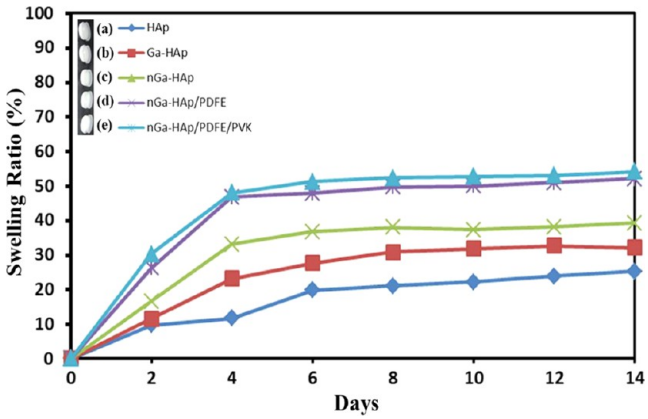

Figure 10. Swelling ratios of (a) HAp, (b) Ga-HAp, (c) nGa-HAp, (d) nGa-HAp/PDFE, and (e) nGa-HAp/PDFE/PVK composites at 0, 2, 4, 6, 8, 10, 12, and 14 days of immersion in SBF.

to 25% for HAp, 32% for Ga-HAp, 39% for nGa-HAp, 51% for nGa-HAp/PDFE, and 52% for nGa-HAp/PDFE/PVK composite during 14 days of immersion and then no significant changes were observed. From the swelling curves, it is inferred that in the presence of neem gum-mediated HAp, the swelling behavior of the composite sample is more significant. The swelling property also increases the surface-to-volume ratio, thus allowing the proliferation of cells and thereby promoting bone growth. It is because of the fact that the swelling property allows the sample to utilize the nutrients from the medium and promote more adhesion property.

Consequently, the degradation behaviors of the as-developed samples (HAp, Ga-HAp, nGa-HAp, nGa-HAp/PDFE, and nGa-HAp/PDFE/PVK composites) are presented in Figure 11. From the result observed, the percentage of degradation for the as-developed nGa-HAp/PDFE/PVK composite was significantly low. It is prominent to note that there occurred an interface between nGa-HAp and PVK, which significantly lowers the degradation ability, thereby ensuring the stability of the composite.

Thus, the as-developed nGa-HAp/PDFE/PVK composite had an optimal property of fair swelling and low degradation,

https://doi.org/10.1021/acsomega.1c02186
ACS Omega 2021, 6, 22537−22550

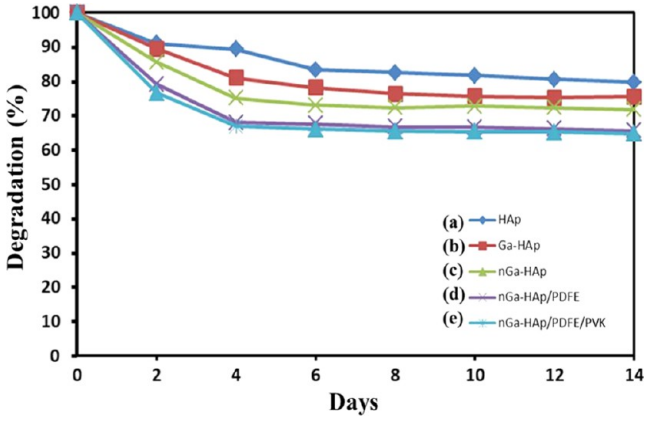

Figure 11. Percent degradation of (a) HAp, (b) Ga-HAp, (c) nGa-HAp, (d) nGa-HAp/PDFE, and (e) nGa-HAp/PDFE/PVK composites at 0, 2, 4, 6, 8, 10, 12, and 14 days of immersion in SBF.

which will be suitable for biomedical applications especially in the field of orthopedics.

CONCLUSIONS

Biocomposite coating based on the nGa-HAp/PDFE/PVK composite over Ti was developed for biomedical applications. The as-developed coating was evaluated for its physiochemical, morphological, mechanical, and biological properties by an array of characterization techniques. The formation of the nGa-HAp/PDFE/PVK composite is well evident from the FT-IR and XRD studies. It is investigated from the HRSEM technique that the biocomposite coating exhibited a uniform, compact morphology with spherical grainlike structures over the surface, which will be an ideal platform for the cell proliferation, whereas the composition of the composite is apparent from the EDS analysis. The hardness value (H_v) observed for the nGa-HAp/PDFE/PVK composite showed high mechanical strength of the as-developed composite, which is due to the presence of the PVK polymer. The higher corrosion potential and lower corrosion current obtained for nGa-HAp/PDFE/PVK composite-coated Ti revealed the corrosion protection performance in the SBF solution. The composite coating exhibited strong activity against Gram-negative bacterial strain *P. aeruginosa*. The presence of Ga^{3+} in the composite plays a key role in providing the antibacterial property. Furthermore, the nontoxic nature of the as-developed nGa-HAp/PDFE/PVK composite coating was tested toward the MG 63 cells and the % cell viability exceeded to 90%, which shows the biocompatible nature of the composite coating. The bioactive nature of the composite-coated Ti is evaluated in physiological body fluid (SBF solution) for 7 and 14 days of immersion, and the formation of apatite at 14 days of incubation reveals the bioactive nature of the as-developed composite coating on Ti. The PDFE aids in improving the bioactive nature of the composite. On considering the obtained results and findings, it can be clearly stated that the as-developed nGa-HAp/PDFE/PVK composite-coated Ti is expected to be a primary choice for bone implant application in the field of orthopedics. Further research on this work is needed for its possible application in clinical trials. Overall, the structural, mechanical, and biological stabilities need to be investigated further on considering the long-term stability of the implants for biomedical applications.

EXPERIMENTAL SECTION

Materials. Biowaste Gastropoda shells, fresh neem (*Azadirachta indica*) gum, gallium nitrate hexahydrate ($Ga(NO_3)_3{\cdot}6H_2O$), diammonium hydrogen phosphate ($(NH_4)_2HPO_4$), poly(*N*-vinylcarbazole) (PVK), ethyl acetate

Scheme 1. Sustainable Route for the Synthesis of nGa-HAp Powder

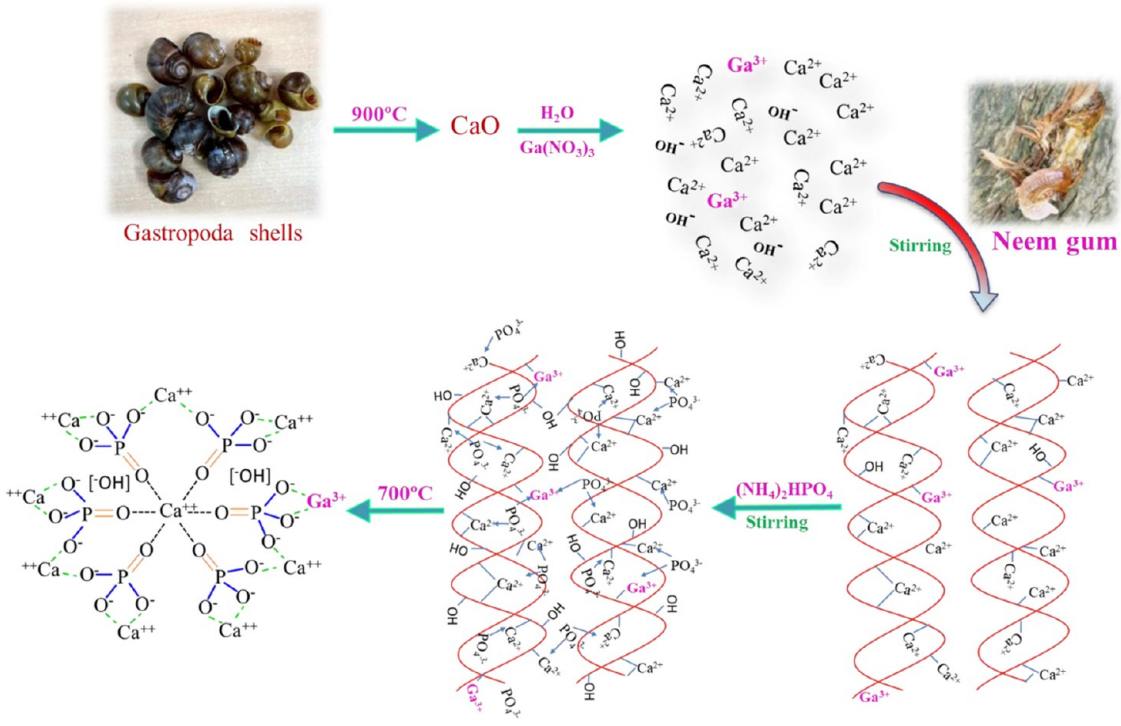

https://doi.org/10.1021/acsomega.1c02186
ACS Omega 2021, 6, 22537−22550

($CH_3COOC_2H_5$), methanol (CH_3OH), and sodium hydroxide (NaOH) as analytical-grade chemicals were purchased from Aldrich Chemicals, India. All of the chemicals and reagents used for these investigations were used as such without any further purification.

Preparation of Plant Fruit Extracts. Healthy and fresh fruits of *Pergularia daemia* (Forsk) were collected from the university campus of Periyar University, Salem District, Tamil Nadu, India. The fruits of *Pergularia daemia* were dried in the shade. The extraction of *Pergularia daemia* from the fruits was carried out according to the standard protocol. In brief, the fruit fiber material was defatted using petroleum ether and then extracted by mixing ethyl acetate and methanol using a Soxhlet apparatus at 40 °C for 72 h. The residue was consequently filtered through Whatman no. 1 filter paper. The ethyl acetate and methanolic extracts of *Pergularia daemia* were further concentrated under vaccum in a rotary vaccum evaporator at 40 °C, and the extract was stored in an amber-colored airtight bottle at 4 °C for further use of composite.

Preparation of PVK Solution. PVK (0.5 g) was dissolved in acetone under magnetic stirring at 80 °C for 1 h and then kept aside for the composite preparation.

Synthesis of nGa-HAp. The synthesis of nGa-HAp using *Azadirachta indica* gum mediator with 0.045 M calcium oxide (CaO), 0.005 M $Ga(NO_3)_2{\cdot}4H_2O$, and 0.03 M $(NH_4)_2HPO_4$ aqueous solutions under magnetic stirring to produce the target (Ca + Ga)/P ratio of 1.67 at room temperature. The synthesis procedure of nGa-HAp is as follows: *Azadirachta indica* gum mediator[21] with 0.045 M CaO was added to 0.005 M $Ga(NO_3)_2{\cdot}4H_2O$ solution and stirred for 3 h. After this step, 0.03 M $(NH_4)_2HPO_4$ solution was added dropwise into the Ca and Ga solution under vigorous magnetic stirring for 24 h and maintained at pH 9 using aqueous ammonia solution, thus yielding a white precipitate.

Then, the acquired white precipitate was reserved in an ultrasonicator at 45 °C for 2 h to ensure the identical mixture, and the sample was dried in a hot-air oven at 80 °C for 3 h. Finally, the dried nGa-HAp powder was washed five times with ethanol and deionized water to eliminate the impurities. Finally, the dried sample of nGa-HAp was then calcined for 24 h and sintered at 700 °C for 5 h and then ground into a fine powder for the preparation of composite (Scheme 1).

Synthesis of the nGa-HAp/PDFE Composite. The nGa-HAp/PDFE composite was prepared through the ultrasonication process using an ultrasonicator (EN-60US (Microplus) at the frequency of 28 kHz and 150 W) in the ratio of 2 g of nGa-HAp in 20 mL of ethanol−water mixture and 20 mL of PDF extract. This mixture was ultrasonicated for 5 h to confirm the excellent dispersion. Finally, the resultant solution is then clearly filtered, washed, and dried for 5 h at 60 °C and then ground to form a powder.

Synthesis of the nGa-HAp/PDFE/PVK Composite. The electrolyte for the electrophoretic deposition was prepared using three different concentrations (0−3 wt %) of the PVK solution and gradually added to a solution of 2 wt % nGa-HAp/PDFE composite in 40 mL of ethanol−water mixture under constant stirring for 5 h. Before deposition, the final mixture of the nGa-HAp/PDFE/PVK composite (0−3 wt % of PVK) was subjected to a strong ultrasonic treatment for 0.5 h to ensure a clear dispersion of the composite into the electrolyte. They were filtered, washed, and dried at 80 °C for 12 h and then ground into a fine powder.

Specimen Preparation. The Ti (with a size of 10 × 10 × 3 mm) sample, which was used as the substrate for the fabrication of the nGa-HAp/PDFE/PVK composite via the electrophoretic deposition technique. Before the deposition, all of the Ti samples were treated with abrasive papers (SiC) from 400 to 1500 grits and polishing suspensions. Finally, the polished Ti samples were cleaned by ultrasonication using distilled water followed by washing with acetone and ethanol mixture for 15 min and drying at room temperature, which was used for the nGa-HAp/PDFE/PVK composite-coating EPD technique.[9]

Electrophoretic Deposition of the nGa-HAp/PDFE/PVK Composite on Ti. During the EPD, a platinum electrode was used as the anode, and the cleaned Ti was used as a cathode (working electrode). The anode and working electrodes were immersed in 100 mL of the nGa-HAp/PDFE/PVK composite suspension while being place parallel to one another with a distance of 4 cm apart. The electrolyte solution for the nGa-HAp/PDFE/PVK composite (0−3 wt % of PVK) deposition was prepared by mixing 3 g of the as-prepared trinary composite in 30 mL of ethanol−water mixture under constant magnetic stirring for 1 h and further uniformly dispersed ultrasonically for about 1 h to obtain a clear dispersion of the electrolyte at room temperature. The electrophoretic deposition of a submicron, homogeneous thick nGa-HAp/PDFE/PVK composite (0−3 wt % of PVK) on the Ti cathode was performed at a constant voltage of 30 V for 10 min using a direct current power supply system. After every successive deposition of composites, the samples were cautiously dragged out of the electrolyte, rinsed with deionized water, dried for 24 h, and kept in a desiccator at room temperature.

Physical Characterizations. Generally, the phase and functional groups of the coating were observed by scraping off the coated material from Ti sample under identical conditions and investigating the resulting powder sample. Fourier transform infrared (FTIR) spectroscopy was employed to determine the presence of various functional groups in HAp, Ga-HAp, nGa-HAp, nGa-HAp/PDFE, and nGa-HAp/PDFE/PVK spectra from 3500 to 500 cm^{-1} using an Impact 400D Nicolet spectrometer by the KBr pellet method.

X-ray diffraction (XRD) patterns of HAp, Ga-HAp, nGa-HAp, nGa-HAp/PDFE, and nGa-HAp/PDFE/PVK were analyzed to confirm the phase compositions using an X-ray diffractometer (XRD, Seifert), and the data were compiled by the International Centre for Diffraction Data (ICDD).

A high-resolution scanning electron microscope (HRSEM, JEOL JSM-6400, Japan) attached with an EDS analyzer was applied to investigate the morphology and presence of elemental composition in the HAp-, Ga-HAp-, nGa-HAp-, nGa-HAp/PDFE-, and nGa-HAp/PDFE/PVK-coated Ti samples.

Vickers Micro-Hardness Test. The micro-hardness of the HAp, Ga-HAp, nGa-HAp, nGa-HAp/PDFE, and nGa-HAp/PDFE/PVK composite-coated Ti samples, respectively, was measured using an Akashi AAV-500 series hardness tester (load 490.3 mN for a dwell time of 20 s, Kanagawa, Japan). The Vickers micro-hardness (H_v) measurements were performed for each sample by taking average of five measurements made at various sites.

Corrosion Resistance of the Coatings. The corrosion tests of blank and Ga-HAp-, nGa-HAp-, nGa-HAp/PDFE-, and nGa-HAp/PDFE/PVK-coated Ti samples were carried out in

https://doi.org/10.1021/acsomega.1c02186
ACS Omega 2021, 6, 22537−22550

simulated body fluid (SBF) solution at room temperature (37 °C) by the potentiodynamic polarization technique. For this investigation, a characteristic Ti sample, a saturated calomel electrode (SCE), and a platinum plate were used as the working, reference, and counter electrodes, respectively, which was used to perform the corrosion experiments using the electrochemical workstation CHI 760C (CH Instruments).

The polarization curves were recorded at the open-circuit potential (OCP), after 1 h of immersion of the blank Ti metal in the SBF solution, and the time to reach a stable open-circuit potential was limited to 1 h owing to the fact that Ti surface may be changed within a longer duration. The potentiodynamic polarization studies of blank and Ga-HAp-, nGa-HAp-, nGa-HAp/PDFE-, and nGa-HAp/PDFE/PVK-coated Ti samples were performed under OCP condition from −0.8 to 0.4 V at a constant scan rate of 1 mV/s. To confirm the reproducibility and reliability of the polarization results, the test was carried out three times and plots were recorded using CHI 760C software.

Antibacterial Activity. The *in vitro* antibacterial activity of the as-developed Ga-HAp, nGa-HAp, nGa-HAp/PDFE, and nGa-HAp/PDFE/PVK composite samples were evaluated against two bacterial species, Gram-negative strain *Pseudomonas aeruginosa* (*P. aeruginosa*) and Gram-positive strain *Staphylococcus aureus* (*S. aureus*), using the agar disk-diffusion technique and minimum inhibitory concentration (MIC). *P. aeruginosa* and *S. aureus* are the most common pathogens associated with biomaterial-centered infections. The stock solution for both the organisms (1×10^8 CFU/mL) was prepared by mixing 1 mL of bacterial solution separately with 9 mL of broth (Luria−Bertani) and then incubated with shaking at 250 rpm for 24 h at 37 °C. The nutrient agar plates were prepared, and the cultures were inoculated for disk-diffusion technique. The sterile paper disks with 5 mm diameter were dipped in Ga-HAp, nGa-HAp, nGa-HAp/PDFE, and nGa-HAp/PDFE/PVK composite samples. Each sample was taken at concentrations of 50 and 100 μg/mL and placed in the agar plate and incubated at 37 °C for a period of 24 h. After the incubation period, the Petri plates were observed for antimicrobial activity based on the width of zone around the disks of each sample.

***In Vitro* Cell Viability Test.** Human osteosarcoma MG63 cells (HOS MG63, ATCC CRL-1427TM) were cultivated in sterile tissue culture flasks containing extraction medium, Dulbecco's modified Eagle's medium (DMEM) supplied with 1% penicillin-streptomycin, and 10% fetal bovine serum at 37 °C in a humidified atmosphere containing 5% CO_2, and the MG 63 cells were passaged by trypsinization before confluence. The measurements were performed using an indirect method in which the immersion extracts were used to culture for the investigation of cell viability of the nGa-HAp/PDFE/PVK-coated Ti samples. Before the measurements, nGa-HAp/PDFE/PVK-coated Ti samples were sterilized under ultraviolet light during the cross-linking process.

To evaluate the cytotoxicity of the nGa-HAp/PDFE/PVK-coated Ti samples, HOS MG63 cells were seeded in 12-well plates at 10^4 cells/mL by measuring the mitochondrial dehydrogenase activity using a modified 3-(4,5-dimethyl-2-tiazolyl)-2,5-diphenyl-2-tetrazolium bromide (MTT) assay. The immersion extracts were collected from 20 mL of DMEM in a humidified atmosphere with 5% CO_2 at 37 °C at different concentrations for 0.5, 5, 50, 100, and 150 μg. MG63 cells were seeded in 12-well plates with a density of at 10^4 cells per well in 50 μL of medium. For all samples, viability images were taken from at least three to five different locations to attain an overview of the cell attachments on the nGa-HAp/PDFE/PVK composite-coated Ti samples. The absorbance of the samples was measured with a multimode detector at a wavelength of 570 nm, and the cell viability (%) of the nGa-HAp/PDFE/PVK-coated Ti samples was calculated with respect to control wells using the following formula

$$\%\ \text{cell viability} = [\text{A}]\text{test}/[\text{A}]\text{control} \times 100$$

***In Vitro* Bioactivity in SBF.** The *in vitro* bioactivity of the nGa-HAp/PDFE/PVK composite-coated Ti samples was tested by soaking in 30 mL of Kokubo's simulated body fluid[46] (SBF) in a beaker with an airtight lid for 7 and 14 days at 37 °C. After the formation of apatite layer at time periods of 7 and 14 days, the immersed samples were taken out and gently rinsed in deionized water. The bonelike apatite formed on the nGa-HAp/PDFE/PVK composite-coated Ti samples was air-dried before the investigation by FESEM analysis.

Swelling Behaviors in SBF. Absorption is the most significant process, and for this purpose, the swelling study is performed, which reveals the stability of the samples. The as-developed samples (HAp, Ga-HAp, nGa-HAp, nGa-HAp/PDFE, and nGa-HAp/PDFE/PVK composites) were subjected to swelling test. The samples were soaked in 10 mL of SBF solution, which was prepared according to Kokubo's protocol.[46] The swelling test was performed for all of the samples on different days (0, 2, 4, 6, 8, 10, 12, and 14 days) of immersion. All of the samples were weighed before and after immersion. The immersed samples were removed, and the adsorbed solution was removed by air drying at 36 °C, and then the samples were weighed. The difference in the weight of the samples before and after immersion was calculated in terms of swelling percentage (%) as follows:[47]

$$\text{swelling ratio}\ (\%) = \frac{W_\text{w} - W_\text{d}}{W_\text{d}} \times 100$$

where W_w and W_d are the wet and dry weights of the samples, respectively. The experiment was performed in triplicate to estimate the swelling behavior, and the average was taken.

Degradation Behaviors in SBF. The as-developed samples were immersed in SBF solution for different days (0, 2, 4, 6, 8, 10, 12, and 14 days) to investigate its degradation behavior. The weight of each sample was measured before the immersion and noted. After the specific time period, the samples were carefully removed and weighed. The degradation ability of the samples was calculated by adopting the following equation:[47]

$$\text{degradation}(\%) = \frac{W_\text{d}}{W_\text{o}} \times 100$$

where D is the degradation ability in %, and W_o and W_d are the weights of the sample before and after degradation, respectively. The test was performed three times and the average of the obtained values was taken.

Statistical Analysis. The biological data are evaluated using statistical analysis by one-way analysis of variance (ANOVA, Tukey's test for a post hoc examination). The antibacterial activity data are represented as mean ± standard deviation. The difference observed between samples was considered to be statistically significant probability values of $P < 0.05$.

https://doi.org/10.1021/acsomega.1c02186
ACS Omega 2021, 6, 22537−22550

AUTHOR INFORMATION

Corresponding Author

Gopi Dhanaraj − *Department of Chemistry, Periyar University, Salem 636 011 Tamil Nadu, India;* orcid.org/0000-0001-6662-1238; Email: dhanaraj_gopi@yahoo.com

Authors

Saravanakumar Ponnusamy − *Department of Chemistry, Periyar University, Salem 636 011 Tamil Nadu, India*

Ramya Subramani − *Department of Physics, School of Basic and Applied Sciences, Central University of Tamil Nadu, Thiruvarur 610 101 Tamil Nadu, India*

Shinyjoy Elangomannan − *Department of Physics, School of Basic and Applied Sciences, Central University of Tamil Nadu, Thiruvarur 610 101 Tamil Nadu, India*

Kavitha Louis − *Department of Physics, School of Basic and Applied Sciences, Central University of Tamil Nadu, Thiruvarur 610 101 Tamil Nadu, India*

Manoravi Periasamy − *Materials Chemistry and Metal Fuel Cycle Group, Indira Gandhi Centre for Atomic Research, Kalpakkam 603102 Tamil Nadu, India*

Complete contact information is available at: https://pubs.acs.org/10.1021/acsomega.1c02186

Notes

The authors declare no competing financial interest.

ACKNOWLEDGMENTS

G.D. acknowledges the major financial support from the University Grants Commission-Department of Atomic energy (UGC-DAE CSR, ref No. CSR-KN/CRS-118/2018-19/1056, Dated: 26.12.2018) and Department of Science and Technology (DST-SERB, Ref no. EMR/2017/003803). R.S. (F.4-2/2006(BSR)/CH/17-18/0170, Dated: 25.09.2018) and S.E. (No. F.4-2/2006 (BSR)/CH/18-19/0078; Dated: 06-02-2019) acknowledge the University Grants Commission for Dr. D.S. Kothari Fellowship, New Delhi, India.

ABBREVIATIONS

nGa-HAp, nano-gallium-substituted hydroxyapatite; PDFE, *Pergularia daemia* fiber extract; PVK, poly(*N*-vinylcarbazole); Ti, titanium; MTT, (3-(4,5-dimethyl-2-tiazolyl)-2,5-diphenyl-2-tetrazolium bromide); EPD, electrophoretic deposition; OCP, open-circuit potential; FTIR, Fourier transform infrared; XRD, X-ray diffraction; HRSEM, high-resolution scanning electron microscopy; EDS, energy-dispersive spectroscopy; DMEM, Dulbecco's modified Eagle's medium

REFERENCES

(1) Karunakaran, G.; Eun, B. C.; Govindan, S. K.; Evgeny, K.; Dmitriy, Y. K.; Janarthanan, G.; Mamatha, M. P.; Rajendran, S.; Selvakumar, B.; Mikhail, V. G. Sodium dodecyl sulfate mediated microwave synthesis of biocompatible super para magnetic mesoporous hydroxyapatite nanoparticles using black Chlamys varia seashell as a calcium source for biomedical applications. *Ceram. Int.* **2019**, *45*, 15143−15155.

(2) Jia, Z.; Wenhao, Z.; Jianglong, Y.; Pan, X.; Hui, G.; Yan, C.; Yufeng, Z. Constructing Multilayer Silk Protein/Nanosilver Biofunctionalized Hierarchically Structured 3D Printed Ti6Al4 V Scaffold for Repair of Infective Bone Defects. *ACS Biomater. Sci. Eng.* **2019**, *5*, 244−261.

(3) Ullah, I.; Muhammad, A. S.; Hui, L.; Sharafadeen, K. K.; Ji, Z.; Shuyuan, Z.; Ling, R.; Ke, Y. Mechanical, Biological, and Antibacterial Characteristics of Plasma Sprayed (Sr, Zn) Substituted Hydroxyapatite Coating. *ACS Biomater. Sci. Eng.* **2020**, *6*, 1355−1366.

(4) Ghosh, R.; Oliver, S.; Sabrina, W.; Benjamin, L. M.; Matthew, Z. Y. Antibacterial Copper-Hydroxyapatite Composite Coatings via Electrochemical Synthesis. *Langmuir* **2019**, *35*, 5957−5966.

(5) Gopi, D.; Shinyjoy, E.; Karthika, A.; Nithiya, S.; Kavitha, L.; Rajeswari, D.; Tingting, T. Single Walled Carbon Nanotubes Reinforced Mineralized Hydroxyapatite Composite Coatings on Titanium for Improved Biocompatible Implant Applications. *RSC Adv.* **2015**, *5*, No. 36766.

(6) Mathi, D. B.; Karthika, R.; Bharathi, P. A.; Mydhili, A.; Gopi, D.; Kavitha, L. Fabrication And Characterization Of Cerium Substituted Hydroxyapatite/Polyvinyl Pyrrolidone Coating On Ti-6al-4v Alloy For Orthopedic Applications. *Adv. Nat. Appl. Sci.* **2017**, *11*, 111−115.

(7) Gopi, D.; Shinyjoy, E.; Kavitha, L. Influence of Ionic Substitution in Improving the Biological Property of Carbon Nanotubes Reinforced Hydroxyapatite Composite Coating on Titanium for Orthopedic Applications. *Ceram. Int.* **2015**, *41*, 5454−5463.

(8) Elangomannan, S.; Kavitha, L.; Bhagyamathi, D.; Venkata, S. K.; Kannan, S.; Gopi, D. Carbon Nanofiber/Polycaprolactone/Mineralized Hydroxyapatite Nanofibrous Scaffolds for Potential Orthopedic Applications. *ACS Appl. Mater. Interfaces* **2017**, *9*, 6342−6355.

(9) Karthika, A.; Kavitha, L.; Surendiran, M.; Kannan, S.; Gopi, D. Fabrication of divalent ion substituted hydroxyapatite/gelatin nanocomposite coating on electron beam treated titanium: mechanical, anticorrosive, antibacterial and bioactive evaluations. *RSC Adv.* **2015**, *5*, 47341−47352.

(10) Shiba, K.; Satoshi, M.; Tadashi, Y.; Nobuhiro, O.; Yuichi, O.; Kiyoshi, O.; Takuya, K.; Motohiro, T. Effect of Cationic Surfactant Micelles on Hydroxyapatite Nanocrystal Formation: An Investigation into the Inorganic−Organic Interfacial Interactions. *Cryst. Growth Des.* **2016**, *16*, 1463−1471.

(11) Gopi, D.; Nithiya, S.; Shinyjoy, E.; Rajeswari, D.; Kavitha, L. Carbon Nanotubes/Carboxymethyl Chitosan/Mineralized Hydroxyapatite Composite Coating on Ti-6Al-4V Alloy for Improved Mechanical and Biological Properties. *Ind. Eng. Chem. Res.* **2014**, *53*, 7660−7669.

(12) Ronan, K.; Bobby, M. B. Novel Sustainable Route for Synthesis of Hydroxyapatite Biomaterial from Biowastes. *ACS Sustainable Chem. Eng.* **2017**, *5*, 2237−2245.

(13) Chen, J.; Zhenliang, W.; Shengnan, Z. Z. W.; Jiulin, W.; Qiqing, Z.; et al. Synthesis of Hydroxyapatite Nanorods from Abalone Shells Via Hydrothermal Solid-State Conversion. *Mater. Des.* **2015**, *87*, 445−449.

(14) Saxon, E. S. Solute Composition: A Parameter Affecting the Distribution of Freshwater Gastropods *Spring-Fed Wetlands: Important Scientific and Cultural Resources of the Intermountain Region* 2002, *775*, 674 7006.

(15) Sathishkumar, S.; Kavitha, L.; Shinyjoy, E.; Gopi, D. Tailoring the Sm/Gd-Substituted Hydroxyapatite Coating on Biomedical AISI 316L SS: Exploration of Corrosion Resistance, Protein Profiling, Osteocompatibility, and Osteogenic Differentiation for Orthopedic Implant Applications. *Ind. Eng. Chem. Res.* **2016**, *55*, 6331−6344.

(16) Fang, W.; Hong, Z.; Jianwei, Y.; Boguang, Y.; Yabin, Z.; Junjie, L.; Fanglian, Y. Hydroxyapatite Crystal Formation in the Presence of Polysaccharide. *Cryst. Growth Des.* **2016**, *16*, 1247−1255.

(17) Gopi, D.; Kanimozhi, K.; Bhuvaneshwari, N.; Indira, J.; Kavitha, L. Novel Banana Peel Pectin Mediated Green Route for the Synthesis of Hydroxyapatite Nanoparticles and their Spectral Characterization. *Spectrochim. Acta, Part A* **2014**, *118*, 589−597.

(18) Velusamy, P.; Jayabrata, D.; Raman, P.; Baskaralingam, V.; Kannaiyan, P. Greener Approach for Synthesis of Antibacterial Silver Nanoparticles Using Aqueous Solution of Neem Gum (Azadirachta Indica L.). *Ind. Crops Prod.* **2015**, *66*, 103−109.

(19) Gopi, D.; Bhuvaneshwari, N.; Indira, J.; Kavitha, L. Synthesis and spectroscopic investigations of hydroxyapatite using a green chelating agent as template. *Spectrochim. Acta, Part A* **2013**, *104*, 292−299.

(20) Gopi, D.; Kanimozhi, K.; Kavitha, L. Opuntia ficus indica peel derived pectin mediated hydroxyapatite nanoparticles: Synthesis, spectral characterization, biological and antimicrobial activities. *Spectrochim. Acta, Part A* **2015**, *141*, 135−143.
(21) Ponnusamy, S.; Sutha, S.; Kavitha, L.; Manoravi, P.; Gopi, D. An Innovative Azadirachta Indica Gum-Mediated Synthesis of Cocoon-Shaped Nano-AgHAp from Lamellidens Marginalis Shells. *Int. J. Appl. Ceram. Technol.* **2020**, *17*, 2008−2016.
(22) Kandori, K.; Satoko, T.; Wakamura, M.; Fukusumi, M.; Morisada, Y. Effects of Modification of Calcium Hydroxyapatites by Trivalent Metal Ions on the Protein Adsorption Behavior. *J. Phys. Chem. B.* **2010**, *114*, 2399−2404.
(23) Gopi, D.; Sathishkumar, S.; Karthika, A.; Kavitha, L. Development of Ce^{3+}/Eu^{3+} Dual-Substituted Hydroxyapatite Coating on Surgical Grade Stainless Steel for Improved Antimicrobial and Bioactive Properties. *Ind. Eng. Chem. Res.* **2014**, *53*, 20145−20153.
(24) Prabakaran, S.; Rajan, M.; Lv, C.; Guolin, M. Lanthanides-Substituted Hydroxyapatite/Aloe vera Composite Coated Titanium Plate for Bone Tissue Regeneration. *Int. J. Nanomed.* **2020**, *15*, 8261−8279.
(25) Ricardo, D. S. S.; Marcos, V. S. R. Atomistic Simulation of Intrinsic Defects and Trivalent and Tetravalent Ion Doping in Hydroxyapatite. *Adv. Condens. Matter Phys.* **2014**, 1−8.
(26) Mellier, C.; Franck, F.; Verena, S.; Philippe, D.; Mathieu, A.; Sophie, Q.; Dominique, M.; Jean, M. B.; Bruno, B.; Pascal, J. Characterization and Properties of Novel Gallium-Doped Calcium Phosphate Ceramics. *Inorg. Chem.* **2011**, *50*, 8252−8260.
(27) Kurtjak, M.; Marija, V.; Andraz, K.; Lovro, K.; Boris, T.; Danilo, S. Designing Ga(III)-Containing Hydroxyapatite with Antibacterial Activity. *RSC Adv.* **2016**, *6*, 112839−112852.
(28) Kolmas, J.; Ewa, G.; Dagmara, K. R. Substituted Hydroxyapatites with Antibacterial Properties. *BioMed Res. Int.* **2014**, No. 178123.
(29) Pajor, K.; Lukasz, P.; Anna, Z.; Urszula, P.; Joanna, K. Modifications of Hydroxyapatite by Gallium and Silver Ions-Physicochemical Characterization, Cytotoxicity and Antibacterial Evaluation. *Int. J. Mol. Sci.* **2020**, *21*, 5006−5021.
(30) Melnikov, P.; Mariade, F. C. M.; Augustin, M.; Andre, R. T.; Diogo, M. A. Evaluation of in vitro Toxicity of Hydroxyapatite Doped with Gallium. *Mater. Lett.* **2019**, *253*, 343−345.
(31) Jabli, M.; Najeh, T.; Khiari, R.; Tawfik, A. S. Physicochemical Characteristics and Dyeing Properties of Lignin-Cellulosic Fibers Derived from Nerium Oleander. *J. Mol. Liq.* **2018**, *249*, 1138−1144.
(32) Govindarajan, M.; Giovanni, B. One-Pot Green Synthesis of Silver Nanocrystals Using Hymenodictyon Orixense: A Cheap and Effective Tool Against Malaria, Chikungunya and Japanese Encephalitis Mosquito Vectors? *RSC Adv.* **2016**, *6*, 59021−59029.
(33) Sridevi, S.; Sutha, S.; Kavitha, L.; Gopi, D. Physicochemical and Biological Behaviour of Biogenic Derived Hydroxyapatite and Carboxymethyl Cellulose/Sodium Alginate Biocomposite Coating on Ti6Al4V Alloy for Biomedical Applications. *Mater. Chem. Phys.* **2020**, No. 123455.
(34) Bhavina, V.; Ruchia, V.; Santani, D. D. Diuretic Potential of Whole Plant Extracts of Pergularia daemia (Forsk.). *Iran. J. Pharm. Res.* **2011**, *10*, 795−798.
(35) Vaithiyanathan, V.; Sankaran, M. Assessment of anticancer activity: A comparison of dose−response effect of ethyl acetate and methanolic extracts of Pergularia daemia (Forsk). *Oral Sci. Int.* **2016**, *13*, 24−31.
(36) Mir, A. S.; Mahmood, D.; Shabeer, A.; et al. Analysis of Phytochemistry and Antimicrobial activity of Tridax procumbens Linn. *Chem. Sci. J.* **2016**, *7*, 1000132.
(37) Bhaskar, V. H.; Balakrishnan, N. Veliparuthi (Pergularia daemia (Forsk.) Chiov.) − As a phytomedicine: A review. *Int. J. PharmTech Res.* **2009**, *1*, 1305−1313.
(38) Ahmed, F.; Catherine, M. S.; Regina, A. M. V.; Maria, C. R. T.; Rigoberto, A.; Debora, F. R. Antimicrobial Applications of Electroactive PVK-SWNT Nanocomposites. *Environ. Sci. Technol.* **2012**, *46*, 1804−1810.
(39) Grigoras, A. G. A review on medical applications of poly(N-vinylcarbazole) and its derivatives. *Int. J. Polym. Mater. Polym. Biomater.* **2016**, *65*, 888−900.
(40) Aleshin, A. N.; Igor, P. S.; Alexei, S.; Vasily, N. P.; Irina, N. T. Poly(9-vinylcarbazole)−graphene oxide composite field-effect transistors with enhanced mobility. *Org. Electron.* **2014**, *16*, 186−194.
(41) Gopi, D.; Karthika, A.; Sekar, M.; Kavitha, L.; Pramod, R.; Jishnu, D. Development of lotus-like hydroxyapatite coating on HELCDEB treated titanium by pulsed electrodeposition. *Mater. Lett.* **2013**, *105*, 216−219.
(42) Grandfield, K.; Zhitomirsky, I. Electrophoretic deposition of composite hydroxyapatite−silica−chitosan coatings. *Mater. Character.* **2008**, *59*, 61−67.
(43) Raddaha, N.; Luis, C. A.; Sandra, C. P.; Sannakaisa, V.; Judith, A. R.; Aldo, R. B. Electrophoretic Deposition of Chitosan/h-BN and Chitosan/h-BN/TiO2 Composite Coatings on Stainless Steel (316L) Substrates. *Materials* **2014**, *7*, 1814−1829.
(44) Zhang, Y.; Jayarama, R. V.; Adel, E.; Seeram, R.; Bo, S.; Chwee, T. L. Electrospun Biomimetic Nanocomposite Nanofibers of Hydroxyapatite/Chitosan for Bone Tissue Engineering. *Biomaterials* **2008**, *29*, 4314−4322.
(45) Huang, Y.; Guiqin, S.; Xiaotong, C.; Zhenhui, W.; Xuejiao, Z.; Shuguang, H.; Zhuobin, S.; Hejie, Y.; Dongdong, Y.; Xiaojun, Z. Nanostructured Ag^{+}-Substituted Fluorhydroxyapatite-TiO_2 Coatings for Enhanced Bactericidal Effects and Osteoinductivity of Ti for Biomedical Applications. *Int. J. Nanomed.* **2018**, *13*, 2665−2684.
(46) Kokubo, T.; Takafama, H. *Biomaterials* **2006**, *27*, 2907−2915.
(47) Trakoolwannachai, V.; Kheolamai, P.; Ummartyotin, S. Characterization of hydroxyapatite from eggshell waste and polycaprolactone (PCL) composite for scaffold material. *Composites, Part B* **2019**, *173*, No. 106974.

https://doi.org/10.1021/acsomega.1c02186
ACS Omega 2021, 6, 22537−22550